4-21-2014

Anisotropic thermal expansion in molecular solids: Theory and experiment on LiBH4

Nikolai A. Zarkevich
Ames Laboratory, zarkev@ameslab.gov

E. H. Majzoub
University of Missouri–St. Louis

Duane D. Johnson
Iowa State University, ddj@iastate.edu

Anisotropic thermal expansion in molecular solids: Theory and experiment on LiBH4

Abstract
We propose a reliable and efficient computational method for predicting elastic and thermal expansion properties in crystals, particularly complex anisotropic molecular solids, and we apply it to the room-temperature orthorhombic Pnmaphase of LiBH4. Using density-functional theory, we find thermal expansion coefficients at finite temperature, and we confirm them by temperature-dependent, *in situ* x-ray diffraction measurements. We also consider the effects of volume and pressure, as well as energy barriers for BH4– rotations and collective motions. Our combined study validates the theory and provides a better understanding of the structural behavior of LiBH4.

Keywords
Materials Science and Engineering

Disciplines
Engineering Physics | Metallurgy

Comments
This article is from *Physical Review B* 89 (2014): 134308, doi:10.1103/PhysRevB.89.134308. Posted with permission.

Anisotropic thermal expansion in molecular solids: Theory and experiment on $LiBH_4$

N. A. Zarkevich,[1,*] E. H. Majzoub,[2,3,†] and D. D. Johnson[1,4,‡]
[1]*The Ames Laboratory, U. S. Department of Energy, Ames, Iowa 50011-3020, USA*
[2]*Center for Nanoscience, Physics and Astronomy, University of Missouri, St. Louis, Missouri 63121, USA*
[3]*Sandia National Laboratories, Livermore, California 94551, USA*
[4]*Materials Science & Engineering, Iowa State University, Ames, Iowa 50011-2300, USA*
(Received 29 August 2013; revised manuscript received 18 February 2014; published 21 April 2014)

We propose a reliable and efficient computational method for predicting elastic and thermal expansion properties in crystals, particularly complex anisotropic molecular solids, and we apply it to the room-temperature orthorhombic *Pnma* phase of $LiBH_4$. Using density-functional theory, we find thermal expansion coefficients at finite temperature, and we confirm them by temperature-dependent, *in situ* x-ray diffraction measurements. We also consider the effects of volume and pressure, as well as energy barriers for BH_4^- rotations and collective motions. Our combined study validates the theory and provides a better understanding of the structural behavior of $LiBH_4$.

DOI: 10.1103/PhysRevB.89.134308 PACS number(s): 05.70.−a, 65.40.De, 61.05.cp, 31.70.Ks

I. INTRODUCTION

Molecular solids constitute a large class of technologically useful materials, composed of complex arrangements of molecular and atomic units. Due to their bonding and structure, which can change under external stress or with temperature, elastic and thermal structural properties can be difficult to predict accurately, especially as molecular solids often have plural local minima in the potential energy surface (PES), yielding nonharmonic vibrations [1–3]. A reliable, generic approach for predicting elasticity and thermal expansion, applicable to simple isotropic crystals and complex anisotropic molecular solids, would be very valuable, if easily implemented in *ab initio* methods. Below we provide such a method and apply it to lithium borohydride ($LiBH_4$).

$LiBH_4$ has been well studied both theoretically [1–9] and experimentally [10–37]. This ionic molecular solid is a widely used reducing agent. As a complex hydride with 18.4 wt. % H, it is considered a promising material for high-capacity hydrogen storage for fuel-cell vehicles [38–49]. $LiBH_4$ has been incorporated into carbon aerogels, and calorimetry measurements indicate that an orthorhombic-to-hexagonal transition occurs at a lower temperature in this mesoporous carbon support structure [50–53]; it also exhibits reversible hydrogen sorption not observed in neat $LiBH_4$. The observed changes in the thermodynamics are striking, and they require a deeper understanding of all solid phases for the development of technologies, including lattice properties, and phase transitions between room and operational temperature.

Thermal expansion has been successfully calculated for metals [54,55] and simple crystals with fixed lattice topology and well-known equations of state (EOSs) [56–59]. One technique widely used to address thermal expansion is the quasiharmonic approximation (QHA) [60], in which the lattice phonon spectra are calculated at several cell volumes. The equilibrium cell volume is obtained by minimizing the Helmholtz free energy ($F = E - TS$), including phonon (harmonic) vibrational entropy at each volume. This may be performed by parametrizing the cell volume in terms of the lattice vectors to calculate the thermal expansion coefficients. This process is computationally intensive as the phonon spectra must be calculated at each volume. For molecular solids, the QHA free energy requires an empirical anharmonic correction [60]. For polymorphic $LiBH_4$ with multiple low-energy structures [61] arising from the "corrugated" PES [1–4], QHA results differ dramatically from experiment [62]; see below.

Here, to predict anisotropic thermal expansion, we offer an efficient alternative method via a polynomial expansion for the PES that is easily implemented using density-functional theory (DFT). We apply it to $LiBH_4$ (Fig. 1), a nontrivial anisotropic molecular solid, and we show excellent agreement with assessed values; we also apply it to metallic Li and ionic LiH (see Appendix A) to show generic applicability. Computational details are given in Appendix B. To predict the structural properties of molecular solids at finite temperature, we study the lattice (Sec. II B) and molecular motions (Appendix C) that determine such behavior. We fully relax the molecular crystal. We then find average lattice constant *distortions* using Boltzmann statistics, and we express their derivatives with respect to pressure and temperature via a polynomial energy expansion (Sec. II). The anisotropic elastic and thermal expansion coefficients can then be directly calculated using DFT methods. We validate and confirm (Sec. III) our theoretical predictions of the thermal expansion by *in situ* x-ray diffraction measurements.

II. THEORY

For complex molecular crystals, such as $LiBH_4$ (strong bonding of BH_4^- is visualized in Fig. 1), in addition to the cell lattice parameters (Table I compares DFT and assessed values), there are multiple internal degrees of freedom (DOF), but not all of them affect the thermal expansion. To predict anisotropic lattice thermal expansion, all the relevant DOF must be addressed, while others (e.g., internal nuclear DOF and strong molecular bonds) can be fixed. Some DOF are

*zarkev@ameslab.gov
†majzoube@umsl.edu
‡ddj@ameslab.gov

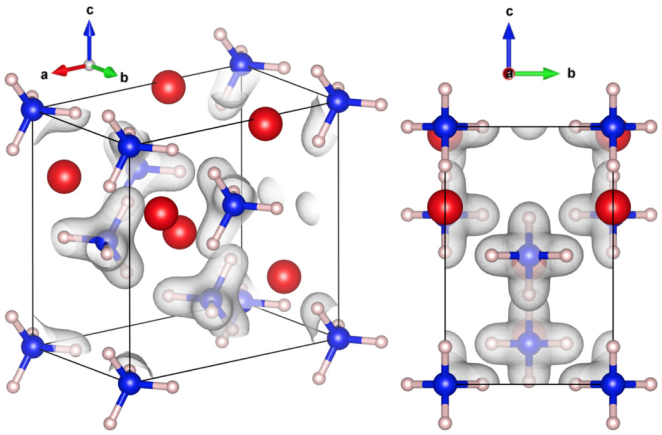

FIG. 1. (Color online) $LiBH_4$ room-temperature orthorhombic $Pnma$ structure with $0.07\,e^-/Å^3$ isosurfaces of electron density around BH_4^- molecular anions. Li is the large red balls, B is the blue, and H is a small white ball attached to a BH bond.

responsible for anharmonic vibrations that affect the structural stability and thermal behavior of the crystal, whereas the internal molecular DOF (which yield the high-frequency harmonic vibrations) contribute to the entropy but cancel in free-energy differences [1], because they are unchanged with allotropic transitions or small structural deviations (e.g., due to thermal expansion).

Here, we establish a numerically reliable approach to calculate the thermal expansion coefficients for complex anisotropic molecular crystals. We first present our general method (Sec. II A), and then we explain the necessity for each constraint imposed on internal DOF, using $LiBH_4$ as an example (Sec. II B). To improve numerical accuracy, we restrict the internal DOF associated with molecular motions, and thus eliminate the nonsystematic errors arising from molecular relaxations, and we replace them with systematic ones, which are then canceled when subtracted for required energy differences.

While derivation of Eq. (3) from Eq. (1) for a one-atom-per-cell simple crystal is in textbooks [65,66], our method is, in fact, general. In Appendix A, we modify the method for materials with known EOS, apply it to simple crystals (namely, to metallic Li and to ionic LiH), and show excellent agreement with experiment. Computational details are given in Appendix B. To justify the approximation of fixed molecular orientations in Sec. II A(b), in Appendix C we compute the rotational barriers [2,4] for $[BH_4]^-$ anions in $LiBH_4$.

TABLE I. Structural parameters (in Å) of $LiBH_4$ for the orthorhombic $Pnma$ and hexagonal $P6_3mc$ phases. Hexagonal structure can be viewed as orthorhombic with $a = b\sqrt{3}$. Unless otherwise specified, experiments are at room temperature and atmospheric pressure; calculations are at $T = 0$ K and $P = 0$ MPa.

Phase	a	b	c (Å)	Ref.
$Pnma$	7.26	4.38	6.67	our DFT at 0 K
	7.248	4.367	6.559	DFT [61]
	7.1160	4.4056	6.6730	$LiBD_4$ at 10 K [63]
	7.1526	4.4278	6.7933	$LiBD_4$ at 302 K [63]
	7.1856	4.4654	6.8295	our expt. ($P \approx 0$)
	7.1772(6)	4.4461(3)	6.8251(6)	$LiBH_4$ 95% [64]
	7.17858(4)	4.43686(2)	6.80321(4)	$LiBH_4$ at 293 K [12]
$P6_3mc$	7.406786	4.27631(5)	6.94844(8)	$LiBH_4$ at 408 K [12]
New GS	8.484	4.348	5.750	DFT [61]

A. Method: Thermal expansion from *ab initio* energy calculations

We generalize the well-established method [65,66] for anisotropic molecular crystals (containing N atomic and molecular ions in a unit cell) using the following approximations, simplifications, and restrictions, imposed after full relaxation of the crystal:

(a) Fix the shape of molecular units, as in the rigid molecule approximation [67–72], so that molecules are not deformed during calculation of the dependence of energy on the lattice constants.

(b) Fix the orientation of molecular units according to the symmetry of the crystal, so that its structural phase does not change.

(c) Fix direct lattice coordinates of the centers of mass of atomic and molecular units, thus preserving the crystallographic structure.

(d) Calculate the total energy per unit cell E versus changes in one lattice constant, with all others fixed [e.g., $E(a)$ at fixed b and c].

(e) Fit E versus distortion $\delta = (a/a_0) - 1$ to

$$E(\delta) = E_0 + E_1\delta + \tfrac{1}{2}E_2\delta^2 + \tfrac{1}{3}E_3\delta^3 + O(\delta^4). \quad (1)$$

This cubic polynomial is constructed *locally* (near a single a_0) and is valid only at $\delta \to 0$.

(f) Get elastic constant from the quadratic term E_2,

$$B_a = C_{aa}V_0 = \left.\frac{d^2E(\delta)}{d\delta^2}\right|_{\delta=0} = E_2. \quad (2)$$

(g) Get the linear thermal expansion from $E_3/(E_2)^2$,

$$\alpha_a = \frac{1}{a}\frac{da}{dT} \approx -Nk_B\frac{E_3}{E_2^2}, \quad (3)$$

where $k_B = 8.617\,33 \times 10^{-5}$ eV/K is the Boltzmann constant [see also nonlocal Eq. (A1) in Appendix A].

(h) Compare theoretical and experimental thermal expansion coefficients at the same lattice constants.

Alternatively, if the functional form of the EOS $E(a)$ is known, one can fit it in a range of a, and extract $\alpha(a)$ using Eq. (A1) [which at $\delta = 0$ reduces to Eq. (3)]. Due to thermally expanding $a(T)$, the dependence of $\alpha(a)$ on $a(T)$ also implies its thermal dependence, obtained within the applicability region of the EOS; see Appendix A.

B. Application to $LiBH_4$

Next, we apply this method to $LiBH_4$. Starting from the experimental lattice constants [12] $a = 7.178\,58$, $b = 4.436\,86$, and $c = 6.803\,21$ Å, measured at 293 K (20 °C), we distort one of the lattice vectors (e.g., a), keeping the others (e.g., b and c) fixed, and we fit the energy E versus

distortion $\delta = (a/a_0) - 1$ by a cubic polynomial (1). From the ratio $-E_3/(E_2)^2$, we find the linear thermal expansion coefficient (3), where $N = 8$ is the number of atomic (4 Li^+) and molecular (4 BH_4^-) units per cell.

Without restrictions (a–c), this computational method is straightforward, in principle, but in practice a molecular solid (like $LiBH_4$) has many internal molecular degrees of freedom, and all of them must be fixed for a reliable polynomial fit [Eq. (1)]. Below we fix (a) the *shape* and (b) the *orientation* of BH_4 molecules. Note that the internal vibrations of BH_4 are high-frequency harmonic modes that do not contribute to phase transitions or thermal expansion [1]. We also fix (c) the direct lattice coordinates of the centers of masses of Li^+ and BH_4^- ions. For the heavy ions, this eliminates long-period oscillations of energy due to soft modes and introduces in each undistorted or distorted structure the same systematic error, which is then canceled in energy differences [1].

To understand the necessity of such restrictions (a–c), let us first consider a fit of data with errors from internal atomic relaxations. Moving atoms introduce nonsystematic errors, preventing reliable extraction of the higher-order terms in (1). For example, after unrestricted atomic relaxations we can extract polynomial coefficients up to E_2 (but not E_3) from a fit to noisy data along a or c. The numerical noise arises from small random changes of atomic coordinates from a relaxation.

After atomic relaxation with (b) fixed *orientations* (but relaxed shapes) of BH_4^- anions, we are able to fit the cubic term E_3 along b; see Fig. 2 (inset). [In the chosen unit cell (Fig. 1), the direct lattice coordinates of Li and B atoms along b are either 0 or 1/2; they are fixed by symmetry.] Interestingly, we find that the ratio $(-E_3/E_2^2)$ is close to zero along b; hence, we expect no thermal expansion in this direction. We can also predict positive thermal expansion along a and c, but a new method is needed for a reliable quantitative description. While the trends are clear, the inherent errors in the small energy changes do not permit accurate values of E_3 and thermal expansion α to be obtained from Eqs. (1) and (3).

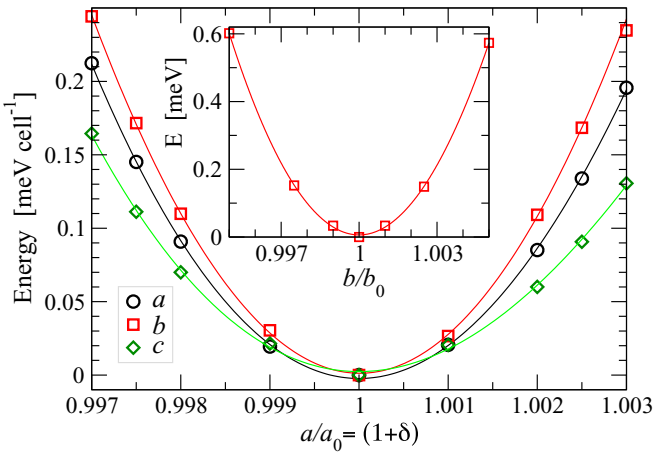

FIG. 2. (Color online) Energy vs cell distortion along a (black circles), b (red squares), and c (green diamonds), with fixed lattice constants in perpendicular directions, calculated from DFT (symbols) and fitted by polynomials in Eq. (1) (lines) with subtracted linear term $E_1\delta$. BH_4^- orientations are fixed. Li and B direct lattice coordinates and BH_4^- shapes are fixed in the main plot (relaxed in the inset).

TABLE II. Polynomial coefficients from Eq. (1).

Coef.	a	b	c	Units
E_2	46	53	36	eV/cell
$-E_3$	325	≈0	300	eV/cell
$-E_3/E_2^2$	0.15	0.0	0.23	eV^{-1} cell

Hence, we employ the method (Sec. II A) to calculate the thermal expansion coefficients in molecular solids. We fix (a) the *shape* (as in the rigid-molecule approximation) [67–72] and (b) the *orientation* of BH_4^- anions; we also fix (c) the *direct lattice coordinates* of the ionic centers of masses. (If BH_4 is not precisely symmetric, we can approximate the BH_4 center of mass by the position of the B nucleus.) By doing so, we fix all internal molecular DOF, turning the associated nonsystematic errors into systematic ones.

Because we are interested only in quadratic and cubic terms of the fitted polynomial, the errors in E_0 and E_1 do not affect our results. To suppress errors originating from the electronic structure, we reduce the allowed error in the total energy specified by the global break condition for the electronic self-consistent loop to 10^{-9} eV. The convergence speed is exponential, and usually we reach desired accuracy in ∼20 electronic steps. We also use a dense $15 \times 23 \times 17$ k-point mesh with ⩾100 points per $Å^{-1}$. We find that the errors are indeed suppressed, and the data points have very small deviations from the smooth polynomial curves (Fig. 2). Comparing energy at $b/b_0 = 1.003$ or 0.997 in Fig. 2 (fixed BH_4) and its inset (relaxed BH_4), one can see that the energy of relaxation of the B-H bonds is also negligible.

We fit 21 energy points along each direction for δ from −2% to 2% in (1), and we extract the elastic constants (2) and linear thermal expansion coefficients (3). The results are presented in Tables II and III. The addition or subtraction of limited data does not substantially change this result. From a comparison of the computed elastic constants, $B_c < B_a < B_b$ (see E_2 in Table II), we find the soft (c) and hard (b) directions. Because $\alpha_c > \alpha_a > \alpha_b \approx 0$, we expect that thermal expansion of c should exceed that of a, while b should change only a little.

Table III compares our extracted theoretical and experimental thermal expansion coefficients for $LiBH_4$ and demonstrates

TABLE III. Thermal expansion coefficients α ($\times 10^{-5}$ K^{-1}) along the lattice vectors from theory and experiment.

a	b	c	T (K)	Ref.
10	0	16	293	DFT [Eq. (3) theory]
9.7	−0.4	15.5	298	Expt. (this work)
9	−2	22	298–353	Expt. (this work, average)
7.2	−2	19	353	Expt. [32]
5.7	0.7	11	298	$LiBH_4$ [32]
−1.1	1.8	4.8	110	$LiBH_4$ [32]
6.2	1.7	1.7	10–302	$LiBD_4$ [39]
8.3	4.3	3	0–300	DFT volume-only method [62]
20	7 ± 7	0 ± 7	0–300	DFT QHA [62]

TABLE IV. Linear thermal expansion coefficients α ($\times 10^{-5}$ K^{-1}), calculated or measured at the same lattice constant a, for metallic Li [73] and ionic LiH [74].

	T (K)	a (Å)	α_{expt}	α_{theor}
Li	200	3.487	3.90	4.07
	250	3.495	4.35	4.14
	300	3.503	4.68	4.21
LiH	298	4.085	4.2	4.32

their good agreement. However, the phonon-based QHA is highly inaccurate for the reasons already mentioned. We also consider metallic Li and ionic LiH, whose atomic coordinates are fixed by lattice symmetry; in these cases, when the EOS functional is known, we provide details in Appendix A for the thermal expansion calculations and comparison to experiment. The method yields excellent agreement with experimental coefficients, without the need to resort to the QHA; see Table IV.

III. EXPERIMENT

As a verification of our present *ab initio* theoretical results, we compare them to the thermal expansion extracted from *in situ* XRD obtained for $LiBH_4$ at Sandia National Laboratories in 2006; see Figs. 3 and 4. Standard $LiBH_4$ powder was purchased from Sigma Aldrich (95% purity) and used without further treatment. The XRD measurements used a Rigaku Rotaflex rotating-anode generator with Cu $K\alpha$ radiation; the diffraction spectra were collected using an Inel 120° curved, position-sensitive detector. The sample was contained in a temperature and atmosphere controlled holder with a Be window in a Bragg-Brentano scattering geometry. The diffraction angles were calibrated using interpolation from a NIST standard silicon powder sample with a resulting resolution of about 0.01° in 2θ. The sample was held under a dynamic vacuum of about 3 Pa. The sample was heated from 300 to 418 K at a rate of about 4 K/min, and then cooled to 300 K, with the XRD pattern recorded every 120 s; see Fig. 3.

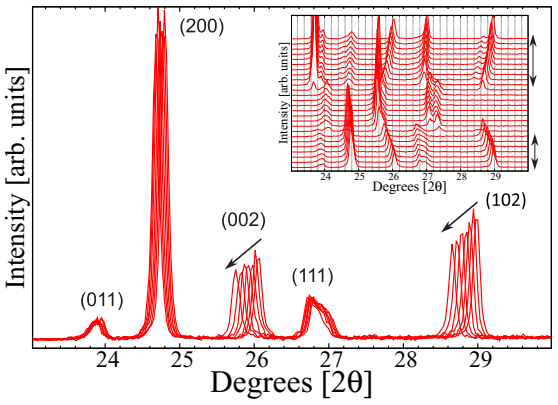

FIG. 3. (Color online) Shift of the XRD peaks vs T. Arrows show a decrease of peak intensity and shift to lower 2θ with increasing T for the (102) and (002) planes. Time-series patterns are shown in the inset (the low-T orthorhombic phase is spanned by arrows). The sample was heated from 300 to 418 K, above the phase transition, and then cooled.

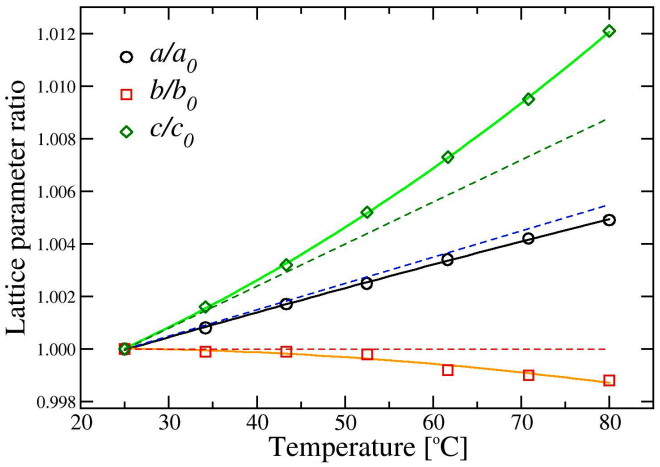

FIG. 4. (Color online) Lattice parameter ratios for a, b, and c axes vs T, relative to the value at 25 °C. Shown are square polynomial fits to the experimental data (solid lines) and calculated α at 20 °C (dashed lines) from Table II.

From our data, we observe a solid-solid phase transition at 381 K, in agreement with the previous measurements [12,13]. Figure 3 shows diffraction spectra for several scans up to, but not surpassing, the transition to the hexagonal phase. The (002) and (102) peaks show a large shift to lower values of 2θ, indicating the expansion along the c axis. Reflections from the (011) and (111) planes remain largely unchanged up to the transition. In addition to the lattice expansion indicated by the peak shifts, the (002) and (102) peaks also show an intensity decrease. Examination of the (002) and (102) planes shows them to be largely hydrogen-containing planes, and the decrease in intensity with rising temperature is in accordance with the Debye-Waller factor.

Our experimentally determined lattice parameter ratios versus temperature are shown in Fig. 4. At the transition temperature, the apparent measured temperature on the external housing of the sample holder was 115 °C, while calorimetry measurements place the transition near 80 °C. Thus, the measured temperature has an offset of about 35 °C. The temperatures shown in Fig. 4 are adjusted values using this offset. From 25 to 80 °C, the fitted (average) thermal expansion coefficients are 9, −2, and 22×10^{-5} K^{-1} for a, b, and c, respectively, and depend very slightly on T. The assessed values at 25 °C (298 K) are compared with our theoretical results and other experiments and calculations in Table III. They agree well with the predicted strain anisotropy and thermal expansion values, also shown in Fig. 4. Due to the clear temperature dependence of the thermal expansion coefficients, theory and experiment should be compared at specific temperatures or matching lattice parameters.

Other *in situ* synchrotron data have been collected on $LiBH_4$ [32,64], but taken at a different pressure (1 atm of argon) with a different scattering geometry (Debye-Scherrer) and lattice parameter standard (NIST LaB_6). Considering

the limited to 95% purity of the powder samples in both experiments, we find the lattice parameter agreement within 1% to be reasonable.

IV. SUMMARY

We proposed a reliable *ab initio* method to predict the elastic and thermal expansion properties for simple and complex crystals. We applied it to the *Pnma* phase of $LiBH_4$, a representative anisotropic molecular solid. We confirmed our theoretical results by comparison to *in situ* XRD measurements; see Fig. 4 and Table III. To reduce numerical errors introduced by the atomic and molecular degrees of freedom, we employed a rigid-molecule approximation with fixed orientation of molecular anions and fixed direct lattice coordinates of the ionic centers of mass. As a result, even in a crystal with molecular complexity, a simple polynomial expansion of energy versus lattice constant distortions accurately describes the elastic constants and thermal expansion coefficients, without requiring phonon calculations. This *ab initio* approach is easily implemented using available DFT methods, and it can be applied to all types of crystals, including ionic molecular solids with anharmonic vibrational modes.

ACKNOWLEDGMENTS

We thank A. V. Smirnov, F. J. Pinski, Y. Filinchuk, and V. Pecharsky for useful discussions. This work was supported by the U.S. Department of Energy, Office of Basic Energy Sciences, Division of Materials Science and Engineering. The research was performed at the Ames Laboratory, which is operated for the U.S. DOE by Iowa State University under Contract No. DE-AC02-07CH11358. Additional support was through the Sandia Metal-Hydride Center of Excellence (DE-FC36-05GO15064). Rotational barriers were calculated at NCSA at the University of Illinois at Urbana-Champaign under NSF (DMR06-0017N).

APPENDIX A: Li AND LiH ISOTROPIC CRYSTALS

Using known dependence $E(a)$ of energy E on the lattice constant a, one can rewrite Eq. (3) in terms of the second and third derivatives:

$$\alpha \approx -\frac{Nk_B}{a}\frac{(\partial^3 E/\partial a^3)}{(\partial^2 E/\partial a^2)^2}. \tag{A1}$$

Any function $E(a)$ of differentiability class C^3 is suitable for use in (A1). Any *analytic* function $E(a)$ can be written in terms of Eq. (1) and equals its Taylor series expansion around any point a_0 in its domain. For such functions, Eqs. (3) and (A1) are equivalent and return the same result at $a = a_0$ (and hence $a/a_0 - 1 \equiv \delta = 0$). However, Eq. (1) is valid *locally*, i.e., only at $\delta \to 0$; hence, Eq. (3) returns a single value $\alpha(a_0)$, estimated at a single point a_0. In contrast, Eq. (A1) returns a function $\alpha(a)$, valid within the whole domain of $E(a)$.

One example of an analytic function $E(a)$ is the isothermal Birch-Murnaghan equation of state [75,76] for cubic ($V = a^3$) crystals,

$$\begin{aligned} E(a) &= E_0 + \tfrac{9}{16}B_0[f^3\,B_0' + f^2\,(2-4f)]a_0^3, \\ \text{with } f &= [(a_0/a)^2 - 1], \\ B_0 &= -V(dP/dV)_{P=0}, \text{and} \\ B_0' &= \quad (dB/dP)_{P=0}. \end{aligned} \tag{A2}$$

Below, we use it to find the thermal expansion coefficients for two isotropic solids, namely metallic Li and ionic LiH.

For Li in the body-centered-cubic [A2] phase ($Im\bar{3}m$, space group no. 229), we fit 37 points at a from 3.333 to 3.539 Å to Eq. (A2), and we obtain $a_0 = 3.442$ Å, $B_0 = 0.0865$ eV/Å^3, and $B_0' = 3.26$. Using Eq. (A1) at $a = 3.503$ Å, we find α is 42.1×10^{-6} K^{-1}, while experiment [73] gives 46.8×10^{-6} K^{-1}; see Table IV.

For LiH with a NaCl-type [B1] lattice ($Fm\bar{3}m$, space group no. 225), we fit 29 points from 3.96 to 4.21 Å to Eq. (A2) and we find $a_0 = 4.016$ Å, $B_0 = 0.0566$ eV/Å^3, and $B_0' = 3.42$. From Eq. (A1), we get $\alpha = 43.2 \times 10^{-6}$ K^{-1} at $a = 4.085$ Å, which compares well with the measured $\alpha = 42 \times 10^{-6}$ K^{-1} and $a = 4.085$ Å at $T = 298$ K (25 °C)[74].

Clearly, our three calculated values for $LiBH_4$ anisotropic molecular crystal, as well as those for metallic Li and ionic LiH, are all in good agreement with experiment; see Tables III and IV.

APPENDIX B: COMPUTATIONAL DETAILS

The Vienna *ab initio* simulation package VASP [77,78] is used to calculate electronic energy, pressure, and atomic forces for instantaneous atomic configurations. We use PAW-GGA [79,80] pseudopotentials, a plane-wave energy cutoff of 700 eV, and a converged k-point mesh [81] including Γ-point for the Brillouin zone integration with at least 75 points per Å^{-1} (e.g., 17 k-points for $b = 4.4$ Å). Atomic and cell relaxations are performed by selective dynamics using a conjugate-gradient algorithm with a Gaussian smearing with $\sigma = 0.05$ eV. The calculated and assessed lattice parameters are compared in Table I. Structural energies are obtained using the tetrahedron method with Blöchl corrections. Calculations of the linear thermal expansion coefficients are preceded by convergence of the atomic forces below 0.001 eV/Å in a fixed unit cell. A dense $15 \times 23 \times 17$ mesh with $\geqslant 100$ k-points per Å^{-1} and the total energy convergence cutoff (EDIFF) of 10^{-9} eV are used within the approximation of rigid BH_4 molecules.

APPENDIX C: ROTATIONAL BARRIERS IN $LiBH_4$

$LiBH_4$ is a molecular solid, consisting of Li^+ cations and BH_4^- molecular anions (Fig. 1). We examine the potential energy barriers of BH_4 molecular rotations using the following method, consisting of three separate computational steps. (a) First, for a single BH_4 motion in a frozen environment, we rotate the molecular unit, keeping all the other atoms fixed in a periodic cell. The cell is chosen to be large enough so that the rotated BH_4 does not interact with its periodic images. (b) Second, after a single BH_4 displacement, we fix the displaced atoms (rotated BH_4) and allow all the other atoms

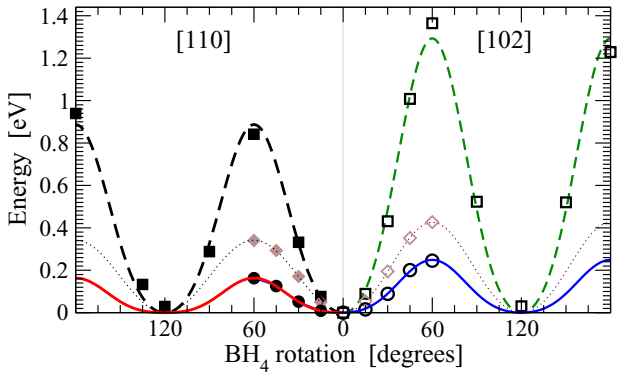

FIG. 5. (Color online) DFT energy of rotation of a single BH_4^- molecule around [110] (left, filled symbols) and [102] (right, empty symbols), calculated by methods (a) (squares, dashed line), (b) (diamonds, dotted line), and (c) (circles, solid line). Lines are fitted to $E(\phi) = E_1 \cos(3\phi) + E_2 \cos(6\phi) - (E_1 + E_2)$, where E_1 and E_2 for method (c) are -82 and 15 meV around [110], and -125 and 17 meV around [102], respectively.

to relax. (c) Third, we again fix all the atoms in the frozen environment used in (a), and we relax the atoms in the rotated BH_4 unit, allowing them to find new equilibrium positions. This energy of displacement of surrounding atoms estimates the "softness" of the local environment. Because relaxations result in energy lowering, barriers in the relaxed environment (b) are lower than those in the frozen environment (a).

Following steps (a)–(c), we calculate potential barriers of rotation for a single BH_4 in both frozen and relaxed local environments. The calculated barriers for BH_4^- rotations, accompanied by collective motion of the surrounding atoms in step (c), are 134 meV (12.9 kJ/mol) and 216 meV (20.7 kJ/mol) around [110] and [102], respectively; see Fig. 5. Nuclear magnetic resonance (NMR) measurements indicate two rotational barriers with activation energies of 16 ± 1 and 20 ± 1 kJ/mol [28] or 17.6 and 24.2 kJ/mol [33], or a single barrier at 20.3(4) kJ/mol [35]. At room temperature, quasielastic neutron scattering measurements are unable to resolve the two modes, and they arrive at an activation energy in pure $LiBH_4$ of about 17 kJ/mol [37]. Other experimentally assessed values include the activation energy of 68 kJ/mol for the hydrogen diffusive motion [82] and the barrier heights of 26.6 and 29.9 kJ/mol assigned to the optic translational and librational modes using a simple harmonic potential in $Pcmn(D_{2h}^{16})$ structure (not $Pnma$), obtained from the inelastic neutron scattering experiment at 77 K [83].

Although the calculated and measured rotational barriers agree, we should add a word of caution. Experimental barriers for BH_4 reorientation are expected to be higher, because one should not expect full relaxations of the surrounding heavier atoms on the time scale of this process. However, those relaxations are included in calculations (b) and (c).

Figure 5 shows that relaxation results in a substantial lowering of the potential energy barriers. Thus, molecular motion must be strongly coupled with motion of the surrounding atoms. This is qualitatively confirmed by the previous calculations [84,85]. In particular, Fig. 1 in [84] shows that increased cation-anion distance substantially lowers the energy of rotated anion, and we show that barrier (b) is lower than (a) in Fig. 5. Method (c) allows rotational relaxations of BH_4^- in a direction perpendicular to the main rotation; a qualitatively similar barrier lowering is shown in Fig. 4 in [84].

Based on our calculations, one can suggest that certain collective rotations of BH_4 units may require little energy. Indeed, the PES is corrugated, and a ground-state (GS) search [61] found other low-energy structures; see Table I. Nevertheless, the rotational barriers in Fig. 5 are high compared to k_BT (26 meV or 2.5 kJ/mol at 300 K); hence, $[BH_4]^-$ molecular units have restricted independent rotational motion in the solid phase. This confirms the validity of the approximation (b) of fixed orientations of $[BH_4]^-$ units, used in Sec. II.

[1] N. A. Zarkevich and D. D. Johnson, Phys. Rev. Lett. **100**, 040602 (2008).
[2] N. A. Zarkevich and D. D. Johnson, Phys. Rev. Lett. **97**, 119601 (2006).
[3] Z. Lodziana and T. Vegge, Phys. Rev. Lett. **97**, 119602 (2006).
[4] Z. Lodziana and T. Vegge, Phys. Rev. Lett. **93**, 145501 (2004).
[5] S. V. Alapati, J. Karl Johnson, and D. S. Sholl, J. Phys. Chem. B **110**, 8769 (2006).
[6] K. Miwa, N. Ohba, S. I. Towata, Y. Nakamori, and S. I. Orimo, Phys. Rev. B **69**, 245120 (2004).
[7] K. Miwa *et al.*, J. Alloys Compd. **404-406**, 140 (2005).
[8] A. A. Gorbik, E. A. Khaikina, A. S. Zyubin, and O. P. Charkin, Zh. Strukt. Khim. **31**, 9 (1990) [J. Struct. Chem. **31**, 856 (1990)].
[9] Yu. B. Kirillov, N. M. Klimenko, and V. G. Zakzhevskii, Zh. Strukt. Khim. **24**, 158 (1983) [J. Struct. Chem. **24**, 469 (1983)].
[10] P. M. Harris and E. P. Meibohm, J. Am. Chem. Soc. **69**, 1231 (1947).
[11] N. C. Hallett and H. L. Johnston, J. Am. Chem. Soc. **75**, 1496 (1953).
[12] J.-P. Soulie, G. Renaudin, R. Cerny, and K. Yvon, J. Alloys Compd. **346**, 200 (2002).
[13] S. Gomes, H. Hagemann, and K. Yvon, J. Alloys Compd. **346**, 206 (2002).
[14] H. Hagemann, S. Gomes, G. Renaudin, and K. Yvon, J. Alloys Compd. **363**, 129 (2004).
[15] G. Renaudin, S. Gomes, H. Hagemann, L. Keller, and K. Yvon, J. Alloys Compd. **375**, 98 (2004).
[16] K. B. Harvey and N. R. McQuaker, Can. J. Chem. **49**, 3282 (1971).
[17] W. D. Davis, L. S. Mason, and G. Stegeman, J. Am. Chem. Soc. **71**, 2775 (1949).
[18] G. W. Ossman and J. W. McGrath, J. Chem. Phys. **47**, 5452 (1967).
[19] I. F. Ferguson, D. R. Masters, B. F. Riley, and M. Turek, Vide Couches Minces **38**, 279 (1983).

[20] K. Wakamori, A. Sawaoka, S. M. Filipek, and B. Baranowski, J. Less-Common Met. (Switzerland) **88**, 217 (1982).
[21] P. J. Herley and W. Jones, Z. Phys. Chem. N. Folge **147**, 147 (1986).
[22] L. Niemela and J. Auranen, Ann. Univ. Turkuensis AI **132**, 3 (1970).
[23] J. Svoboda, Phys. Status Solidi B **70**, K117 (1975).
[24] E. A. Sullivan, J. Less-Common Met. **89**, 214 (1983).
[25] H. Watanabe, T. Totani, M. Ohtsuru, and M. Kubo, Mol. Phys. **14**, 367 (1968).
[26] E. M. Fedneva, V. L. Alpatova, and V. I. Mikheeva, Zh. Neorg. Khim. [Russ. J. Inorg. Chem.] **9**, 826 (1964).
[27] V. E. Gorbunov, K. S. Gavrichev, V. L. Zalukaev, G. A. Sharpataya, and S. I. Bakum, Zh. Neorg. Khim. [Russ. J. Inorg. Chem.] **29**, 1334 (1984).
[28] T. Tsang and T. C. Farrar, J. Chem. Phys. **50**, 3498 (1969).
[29] C. W. Pistorius, Z. Phys. Chem. N. Folge **88**, 253 (1974).
[30] E. Hirota and Y. Kawashima, J. Mol. Spectrosc. **181**, 352 (1997).
[31] K. N. Semenenko, A. P. Chavgun, and V. N. Surov, Zh. Neorg. Khim. [Russ. J. Inorg. Chem.] **16**, 271 (1971).
[32] Y. Filinchuk, D. Chernyshov, and R. Cerny, J. Phys. Chem. C **112**, 10579 (2008).
[33] A. V. Skripov, A. V. Soloninin, Y. Filinchuk, and D. Chernyshov, J. Phys. Chem. C **112**, 18701 (2008).
[34] O. Friedrichs *et al.*, Acta Mater. **56**, 949 (2008).
[35] V. P. Tarasov, S. I. Bakum, V. I. Privalov, and A. A. Shamov, Zh. Neorg. Khim. [Russ. J. Inorg. Chem.] **35**, 1034 (1990).
[36] N. Verdal, T. J. Udovic, and J. J. Rush, J. Phys. Chem. C **116**, 1614 (2012).
[37] N. Verdal, T. J. Udovic, J. J. Rush, X. Liu, E. H. Majzoub, J. J. Vajo, and A. F. Gross, J. Phys. Chem. C **117**, 17983 (2013).
[38] L. Schlapbach and A. Züttel, Nature (London) **414**, 353 (2001).
[39] A. Züttel, P. Wenger, S. Rentsch, P. Sudan, Ph. Mauron, and Ch. Emmenegger, J. Power Sources **118**, 1 (2003).
[40] A. Züttel, S. Rentsch, P. Fischer, P. Wenger, P. Sudan, Ph. Mauron, and Ch. Emmenegger, J. Alloys Compd. **356-357**, 515 (2003).
[41] J. J. Vajo, S. L. Skeith, and F. Mertens, J. Phys. Chem. B **109**, 3719 (2005).
[42] X. B. Yu, D. M. Grant, and G. S. Walker, Chem. Commun. 3906 (2006).
[43] L. Zhou, Renewable Sustainable Energy Rev. **9**, 395 (2005).
[44] Y. Kojima, Y. Kawai, M. Kimbara, H. Nakanishi, and S. Matsumoto, Int. J. Hydrogen Energy **29**, 1213 (2004).
[45] C. Li, P. Peng, D. Zhou, and L. Wan, Int. J. Hydrogen Energy **36**, 14512 (2011).
[46] M. Au and A. Jurgensen, J. Phys. Chem. B **110**, 7062 (2006).
[47] D. K. Ross, Vacuum **80**, 1084 (2006).
[48] L. Laversenne and B. Bonnetot, Ann. Chim., Sci. Mater. (France) **30**, 495 (2005).
[49] Y. Nakamori, S. Orimo, and T. Tsutaoka, Appl. Phys. Lett. **88**, 112104 (2006).
[50] X. Liu, D. Peaslee, C. Z. Jost, and E. H. Majzoub, J. Phys. Chem. C **114**, 14036 (2010).
[51] X. Liu, D. Peaslee, C. Z. Jost, T. F. Baumann, and E. H. Majzoub, Chem. Mater. **23**, 1331 (2011).
[52] A. F. Gross, J. J. Vajo, S. L. Van Atta, and G. L. Olson, J. Phys. Chem. C **112**, 5651 (2008).
[53] D. T. Shane, R. L. Corey, C. McIntosh, L. H. Rayhel, R. C. Bowman, J. J. Vajo, A. F. Gross, and M. S. Conradi, J. Phys. Chem. C **114**, 4008 (2010).
[54] A. A. Quong and A. Y. Liu, Phys. Rev. B **56**, 7767 (1997).
[55] H. M. Jin and P. Wu, J. Alloys Compd. **343**, 71 (2002).
[56] F. Guinea, J. H. Rose, J. R. Smith, and J. Ferrante, Appl. Phys. Lett. **44**, 53 (1984).
[57] P. Vinet, J. R. Smith, J. Ferrante, and J. H. Rose, Phys. Rev. B **35**, 1945 (1987).
[58] P. Abel and G. Bozzolo, Scr. Mater. **46**, 557 (2002).
[59] G. Bozzolo, M. F. del Grosso, and H. O. Mosca, Mater. Lett. **62**, 3975 (2008).
[60] G. Kern, G. Kresse, and J. Hafner, Phys. Rev. B **59**, 8551 (1999).
[61] A. Tekin, R. Caputo, and A. Züttel, Phys. Rev. Lett. **104**, 215501 (2010).
[62] T. J. Frankcombe and G.-J. Kroes, Phys. Rev. B **73**, 174302 (2006).
[63] F. Buchter, Z. Lodziana, P. Mauron, A. Remhof, O. Friedrichs, A. Borgschulte, A. Zuttel, D. Sheptyakov, T. Strassle, and A. J. Ramirez-Cuesta, Phys. Rev. B **78**, 094302 (2008).
[64] J. Lang, A. Gerhauser, Y. Filinchuk, T. Klassen, and J. Huot, Crystals **2**, 1 (2012).
[65] C. Kittel, *Elementary Solid State Physics: A Short Course*, 2nd ed. (Wiley, New York, 1962), eqs. 3.54–56, p. 65.
[66] C. Kittel, *Introduction to Solid State Physics*, 5th ed. (Wiley, New York, 1976).
[67] H. A. Rafizade and S. Yip, J. Chem. Phys. **53**, 315 (1970).
[68] O. A. Usov, Fiz. Tverd. Tela (Leningrad) **16**, 203 (1974) [Phys. Solid State **16**, 203 (1974)].
[69] D. Sahoo and G. Venkataraman, Pramana **5**, 175 (1975).
[70] V. Chandrasekharan and S. H. Walmsley, Mol. Phys. **33**, 573 (1977).
[71] P. Pavlides, D. Pugh, and K. J. Roberts, Mol. Phys. **72**, 121 (1991).
[72] G. M. Day, S. L. Price, and M. Leslie, Cryst. Growth Design **1**, 13 (2001).
[73] W. B. Pearson, Can. J. Phys. **32**, 708 (1954).
[74] D. K. Smith and H. R. Leider, J. Appl. Cryst. **1**, 246 (1968).
[75] F. Birch, Phys. Rev. **71**, 809 (1947).
[76] F. D. Murnaghan, Proc. Natl. Acad. Sci. (U.S.A.) **30**, 244 (1944).
[77] G. Kresse and J. Furthmüller, Phys. Rev. B **54**, 11169 (1996).
[78] G. Kresse and J. Furthmüller, Comput. Mater. Sci. **6**, 15 (1996).
[79] P. E. Blöchl, Phys. Rev. B **50**, 17953 (1994).
[80] J. P. Perdew, J. A. Chevary, S. H. Vosko, K. A. Jackson, M. R. Pederson, D. J. Singh, and C. Fiolhais, Phys. Rev. B **46**, 6671 (1992).
[81] H. J. Monkhorst and J. D. Pack, Phys. Rev. B **13**, 5188 (1976).
[82] R. L. Corey, D. T. Shane, R. C. Bowman, and M. S. Conradi, J. Phys. Chem. C **112**, 18706 (2008).
[83] J. Tomkinson and T. C. Waddington, J. Chem. Soc., Faraday Trans. 2 **72**, 528 (1976).
[84] Z. Lodziana and M. J. van Setten, Phys. Rev. B **81**, 024117 (2010).
[85] A. Remhof, Z. Lodziana, P. Martelli, O. Friedrichs, A. Zuttel, A. V. Skripov, J. P. Embs, and T. Strassle, Phys. Rev. B **81**, 214304 (2010).